

UCLA

UCLA Previously Published Works

Title

Microscale radiosynthesis, preclinical imaging and dosimetry study of [18F]AMBF3-TATE: A potential PET tracer for clinical imaging of somatostatin receptors

Permalink

<https://escholarship.org/uc/item/6wt748kr>

Authors

Lisova, Ksenia
Sergeev, Maxim
Evans-Axelsson, Susan
et al.

Publication Date

2018-06-01

DOI

10.1016/j.nucmedbio.2018.04.001

Peer reviewed



Published in final edited form as:

Nucl Med Biol. 2018 June ; 61: 36–44. doi:10.1016/j.nucmedbio.2018.04.001.

Microscale radiosynthesis, preclinical imaging and dosimetry study of [¹⁸F]AMBF₃-TATE: a potential PET tracer for clinical imaging of somatostatin receptors

Ksenia Lisova^{1,2,3}, Maxim Sergeev^{2,3,5}, Susan Evans-Axelsson^{3,4}, Andreea D. Stuparu^{3,4}, Seval Beykan⁶, Jeffrey Collins^{2,3}, Jason Jones^{1,2,3}, Michael Lassmann⁶, Ken Herrmann^{3,4,7}, David Perrin⁸, Jason T. Lee^{2,3,7,*}, Roger Slavik^{3,4,7,*}, and Michael van Dam^{1,2,3,7,*}

¹Physics in Biology and Medicine Interdepartmental Graduate Program, David Geffen School of Medicine, University of California Los Angeles, Los Angeles, CA, USA

²Crump Institute for Molecular Imaging, David Geffen School of Medicine, University of California Los Angeles, Los Angeles, CA, USA

³Department of Molecular & Medical Pharmacology, David Geffen School of Medicine, University of California Los Angeles, Los Angeles, CA, USA

⁴Ahmanson Translational Imaging Division, David Geffen School of Medicine, University of California Los Angeles, Los Angeles, CA, USA

⁶Department of Nuclear Medicine, University of Würzburg, Würzburg, Germany

⁷Jonsson Comprehensive Cancer Center (JCCC), UCLA, Los Angeles, CA, USA

⁸Department of Chemistry, University of British Columbia, Vancouver, BC, Canada

Abstract

Background—Peptides labeled with positron-emitting isotopes are emerging as a versatile class of compounds for the development of highly specific, targeted imaging agents for diagnostic imaging via positron-emission tomography (PET) and for precision medicine via theranostic applications. Despite the success of peptides labeled with gallium-68 (for imaging) or

*Corresponding authors: R. Michael van Dam, mvandam@mednet.ucla.edu, 4323 CNSI, 570 Westwood Plaza, Los Angeles, CA 90095, USA; Phone: +1-310-206-6507, Roger Slavik, rslavik@mednet.ucla.edu, AR-274 CHS, 10833 Le Conte Avenue, Los Angeles, CA 90095, USA; Phone: +1-310-206-5459, Jason T. Lee, jasontlee@mednet.ucla.edu, 2151 CNSI, 570 Westwood Plaza, Los Angeles, CA 90095, USA; Phone: +1-310-825-7137.

⁵Current address: Department of Radiology, University Hospitals of Cleveland Medical Center, Cleveland, OH, USA.

8 Disclosure

The Regents of the University of California have licensed technology to Sofie Biosciences that was invented by Dr. van Dam, and have taken equity in Sofie Biosciences as part of the licensing transaction. Dr. van Dam is a founder and consultant of Sofie Biosciences. UBC and the BC Cancer Research Agency hold composition of matter patents on the AMBF₃-TATE and on organotrifluoroborate compositions for their use in ¹⁸F-PET; Dr. Perrin is a named inventor on these patents.

9 Ethical approval

Animal studies were approved by the UCLA Animal Research Committee and were carried out according to the guidelines of the Division of Laboratory Animal Medicine at UCLA.

Publisher's Disclaimer: This is a PDF file of an unedited manuscript that has been accepted for publication. As a service to our customers we are providing this early version of the manuscript. The manuscript will undergo copyediting, typesetting, and review of the resulting proof before it is published in its final citable form. Please note that during the production process errors may be discovered which could affect the content, and all legal disclaimers that apply to the journal pertain.

lutetium-177 (for therapy) in the clinical management of patients with neuroendocrine tumors or prostate cancer, there are significant advantages of using fluorine-18 for imaging. Recent developments have greatly simplified such labeling: in particular, labeling of organotrifluoroborates via isotopic exchange can readily be performed in a single-step under aqueous conditions and without the need for HPLC purification. Though an automated synthesis has not yet been explored, microfluidic approaches have emerged for ^{18}F -labeling with high speed, minimal reagents, and high molar activity compared to conventional approaches. As a proof-of-concept, we performed microfluidic labeling of an octreotate analog ($[^{18}\text{F}]\text{AMBF}_3\text{-TATE}$), a promising ^{18}F -labeled analog that could compete with $[^{68}\text{Ga}]\text{Ga-DOTATATE}$ with the advantage of providing a greater number of patient doses per batch produced.

Methods—Both $[^{18}\text{F}]\text{AMBF}_3\text{-TATE}$ and $[^{68}\text{Ga}]\text{Ga-DOTATATE}$ were labeled, the former by microscale methods adapted from manual labeling, and were imaged in mice bearing human SSTR2-overexpressing, rat SSTR2 wildtype, and SSTR2-negative xenografts. Furthermore, a dosimetry analysis was performed for $[^{18}\text{F}]\text{AMBF}_3\text{-TATE}$.

Results—The micro-synthesis exhibited highly-repeatable performance with radiochemical conversion of $50\pm 6\%$ ($n=15$), overall decay-corrected radiochemical yield of $16\pm 1\%$ ($n=5$) in ~ 40 min, radiochemical purity $>99\%$, and high molar activity. Preclinical imaging with $[^{18}\text{F}]\text{AMBF}_3\text{-TATE}$ in SSTR2 tumor models correlated well with $[^{68}\text{Ga}]\text{Ga-DOTATATE}$. The favorable biodistribution, with highest tracer accumulation in the bladder followed distantly by gastrointestinal tissues, resulted in 1.26×10^{-2} mSv/MBq maximal estimated effective dose in human, a value lower than that reported for current clinical ^{18}F - and ^{68}Ga -labeled compounds.

Conclusions—The combination of novel chemical approaches to ^{18}F -labeling and microdroplet radiochemistry have the potential to serve as a platform for greatly simplified development and production of ^{18}F -labeled peptide tracers. Favorable preclinical imaging and dosimetry of $[^{18}\text{F}]\text{AMBF}_3\text{-TATE}$, combined with a convenient synthesis, validate this assertion and suggest strong potential for clinical translation.

Keywords

Tumor-targeting peptide; neuroendocrine tumors; SSTR2 imaging; microfluidic radiochemistry; trifluoroborate; clinical translation; precision medicine

1 Introduction

The use of PET (positron emission tomography) has revolutionized applications in cancer diagnosis. To wit, PET provides dynamic, high-resolution spatio-temporal imaging of tumor uptake and clearance of the injected radiotracer. New hybrid imaging machines, which combine PET with CT (X-ray computed tomography) or MRI (magnetic resonance imaging), can enhance tumor images with the superposition of anatomical features including bony structures, soft-tissues, as well as blood flow for proper anatomical registration and assessment of neovascularization [1].

The production of PET radiotracers requires the judicious use of one of several short-lived positron-emitting nuclides, the choice of which is often dictated in part by the tracer's pharmacokinetics. Of the various PET isotopes in use, fluorine-18, however, is the only one

that can be produced at large scale (>37 GBq [1 Ci] per run) sufficient for production of many patient doses in a single batch. With a moderate half-life, a track-record in FDA approval of ^{18}F -labeled radiotracers, low radiotoxicity, and the highest resolution of any PET nuclide due to a low positron energy [2,3], fluorine-18 is the choice isotope for use in PET. Early on, 2- ^{18}F fluoro-2-deoxy-D-glucose (^{18}F FDG), 3'- ^{18}F fluoro-3'-deoxythymidine (^{18}F FLT), and 1H-1-(3- ^{18}F fluoro-2-hydroxypropyl)-2-nitroimidazole (^{18}F FMISO) [4] enabled cancer imaging based on increased metabolism or hypoxia typical of most but not all cancers. Over the past four decades, ^{18}F FDG has become the most extensively used radiotracer. Yet despite its utility, it typically cannot assess tumor subtypes, and it can give both false negatives and positives [5,6].

Over the past two decades, cancer subtypes are increasingly being distinguished by peptides that have emerged from the study of endocrinology and from various combinatorial screens [7–12] that were undertaken to identify target-based diagnostics and therapeutics [13]. Radiolabeled peptides have been used in clinical PET imaging to distinguish pathologically distinct cell types via recognition of specific molecular targets—a feat that is impossible with ^{18}F FDG [14–17]. Examples of such peptides include octreotate [18–22], bombesin [23], folate [24–29], and RGD [30–32]. Drugs based on peptides include Lupron[™] for prostate cancer, various octreotate analogs (e.g. Sandostatin[™]) for neuroendocrine tumor treatment, the folate-vincristine conjugate Vintafolide[™] for ovarian cancer [33,34], as well as other potential therapeutic toxin conjugates [35,36]. Undeniably, peptides and other relatively large biologic entities provide the needed specificity and affinity for specific recognition of pathognomonic targets, which when properly imaged can enhance personalized diagnosis. In some cases, the same peptide that is used for PET imaging can be engineered for theranostic applications that may include targeted therapy via conjugation/chelation with a radiotoxin, chemotherapeutic, or used fluorescently to guide surgical resections.

Given the molecular complexity of peptides and their general water solubility, peptides have been typically labeled for both diagnostic and radiotherapeutic purposes by radiometal chelation that simply involves heating a peptide-chelator conjugate in the presence of a radiometal (e.g. gallium-68 or copper-64 for imaging or lutetium-177 for therapy). Nevertheless, the use of radiometals for imaging poses several drawbacks, most notably a lack of scalability in their production, the potential for transchelation of the metal *in vivo* [37–39], and generally lower molar activities compared to those labeled with fluorine-18. Yet radiometal chelation remains highly useful for imaging since the production of ^{18}F -labeled peptides continues to be challenged by the relatively short half-life of fluorine-18 (110 min) and more importantly, by both solvent and chemical incompatibilities. Anionic ^{18}F fluoride is unreactive as a nucleophile in water [40] whilst most peptides are insoluble in the dry aprotic solvents that are typically used for ^{18}F -labeling [41], and electrophilic fluorinating agents (e.g. ^{18}F F₂) pose problems including non-selective reaction with cysteine, methionine and tryptophan and generally have lower molar activity compared to anionic ^{18}F fluoride. Hence, multistep syntheses are usually required such as first synthesizing an ^{18}F -labeled prosthetic for further conjugation to a peptide via a variety of chemistries including biorthogonal “click” reactions. While feasible, multistep procedures generally suffer from long reaction times and unwanted side-products. Hence any approach that would simplify radiofluorination would be of considerable interest.

Recently, three new methods for one-step/late-stage ^{18}F -labeling of peptides have appeared: (1) triorganosilyl-fluorides that are labeled by ^{19}F - ^{18}F isotope exchange (IEX) [42,43], (2) NOTA chelation of aluminum-fluoride [44–46], and (3) organoboronate esters to capture aqueous fluoride as ^{18}F -labeled organotrifluoroborates (RBF_3s). While all three methods are relatively simple, peptide- BF_3 bioconjugates are labeled under fully aqueous conditions and do not require HPLC purification. Nevertheless, to date, only a manual synthesis has been reported for various peptide- BF_3 bioconjugates. Moreover, conventional automated radiosynthesizers are not suited to the relatively small reaction volumes needed to achieve high molar activities that can be observed with ^{18}F -labeled peptide- BF_3 conjugates [47]. Hence, emerging microfluidic platforms, which offer advantages such as faster synthesis times, reduced reagent consumption, would be expected to afford the requisite low volumes that in turn would increase molar activity values [48–50] while also increasing both ease of use and access to peptide- BF_3 tracers provided that such a platform could be configured for automated preparation of such conjugates. Our work using electrowetting-on-dielectric (EWOD) microfluidics for the droplet-based radiosynthesis of several ^{18}F -labeled PET tracers (e.g. [^{18}F]FDG, [^{18}F]FLT, [^{18}F]Fallypride) [51–54] has provided compelling evidence that it could be readily adapted to these novel peptide tracers.

To interface the unique microfluidic platform of the EWOD system with an aqueous radiofluorination of a peptide- BF_3 conjugate in a one-step automated synthesis with requisite low volumes, we opted to investigate octreotate as there would be considerable interest if it could be labeled with [^{18}F]fluoride on a microfluidic platform for eventual translation for imaging neuroendocrine tumors (NETs). The previous report on the preclinical evaluation of the ^{18}F -labeled BF_3 -conjugate of octreotate, [^{18}F]AMBF₃-TATE, showed excellent pharmacokinetic properties, with high tumor uptake and high contrast ratios, in mice bearing AR42J tumor xenografts [55] underscoring the potential utility of this particular octreotate-derived tracer. Yet this report featured manual labeling within a fully shielded hot-cell using up to 37 GBq [1.0 Ci] of no-carrier-added [^{18}F]fluoride consistent with clinical GMP guidelines and since then, there has been no report of an automated synthesis of the same tracer, nor a report on microfluidic synthesis, both of which would be of considerable import in terms of extending the means and methods for producing, distributing, and translating this and other ^{18}F -labeled peptide tracers. Our choice for [^{18}F]AMBF₃-TATE is based in part on these previous results that now provide an essential set of benchmarks in terms of radiochemical yields, molar activities, reaction times, tumor uptake values and contrast ratios, all of which arguably would need to be recapitulated on an EWOD microfluidic platform in order to consider its use in clinical translation and a means of comparing microfluidic production compared to a manual synthesis.

In turn, an ^{18}F -labeled octreotate might be expected to compete with [^{68}Ga]Ga-DOTATATE, a DOTA-conjugate to the somatostatin analog octreotide that is now used routinely in the United States to determine target expression and stage neuroendocrine tumors [56] for diagnosis or patient stratification for radioligand therapy using [^{177}Lu]Lu-DOTATATE, a radiotoxin conjugate based on the same targeting peptide. The great success of SSTR2 imaging using the Tyr³-octreotate peptide has paved the way for U.S. FDA approval for Advanced Accelerator Applications (AAA) of NETSPOT, a kit for the preparation of a single patient dose of [^{68}Ga]Ga-DOTATATE injection. Notwithstanding the viability of

[⁶⁸Ga]Ga-DOTATATE, labeling with Ga-68 can make it difficult to meet the high imaging demand at some facilities, while the development of an ¹⁸F-labeled analog, that could be made in larger multi-patient-dose batches is of considerable practical interest.

In this paper, we pave the way toward automated production of such tracers by demonstrating the straightforward radiosynthesis of [¹⁸F]AMBF₃-TATE (Figure 1) in microdroplet format [50]. Eventually, the microfluidic chip could form the basis for a compact, inexpensive synthesis kit. Furthermore, herein we report preclinical imaging studies of human SSTR2 transduced and rat SSTR2 wildtype murine xenografts, performed to provide direct comparison of [⁶⁸Ga]Ga-DOTATATE and [¹⁸F]AMBF₃-TATE in the same animals. To support clinical translation, a dosimetry analysis of [¹⁸F]AMBF₃-TATE is also presented. The microscale synthesis can readily produce clinically-relevant quantities and could be further scaled up using techniques such as concentration of [¹⁸F]fluoride [57] prior to introduction into the microreactor.

2 Materials & Methods

2.1 Reagents and materials

No-carrier-added [¹⁸F]fluoride was produced by the (p,n) reaction of [¹⁸O]H₂O (84% isotopic purity, Zevacor Pharma, Noblesville, IN, USA) in an RDS-112 cyclotron (Siemens; Knoxville, TN, USA) at 11 MeV using a 1 mL tantalum target with havar foil. [¹⁸F]FDG and [⁶⁸Ga]Ga-DOTATATE were obtained from the UCLA Biomedical Cyclotron Facility.

Acetonitrile (MeCN; anhydrous, 99.8%), methanol (MeOH; anhydrous, 99.8%), ethanol (EtOH; 200 proof), aqueous ammonia solution (28% NH₃ in H₂O), and N,N-dimethylformamide (DMF; anhydrous, 99.8%) and 0.2 μm inorganic membrane filters (Whatman Anotop, catalog # 6809-3122) were purchased from Sigma-Aldrich (St. Louis, MO, USA). Saline (0.9% sodium chloride injection, USP) was obtained from Hospira Inc. (Lake Forest, IL, USA); pyridazine (>99%) was obtained from Tokyo Chemical Industry Co., Ltd. (Japan), and hydrochloric acid (HCl; 3N) was obtained from HAZCAT (Mariposa, CA, USA). All reagents were used without further processing or purification. Deionized (DI) water was obtained with a purification system (RODI-C-12BL, Aqua solutions, Inc., Georgia, USA). C18 cartridges (Sep-Pak Plus C18) were obtained from Waters (Milford, MA, USA) and were preconditioned before use by flowing 10 mL of MeOH followed by 15 mL of DI water. The AMBF₃-TATE precursor was prepared as previously described [55].

To prepare a batch of the reaction buffer, 720 μL of pyridazine was added to 5 mL of DMF and 2.5 mL DI water in a 15 mL conical tube. The pH was adjusted to the range 2.0–2.5 with 3M HCl. The final volume was then adjusted with DI water until the final volume reached 10 mL. To prepare a batch of the quench solution (5% NH₃ aq. v/v), 1.8 mL of 28% NH₃ was diluted in 8.2 mL of DI water. pH test strips (0–14 range, Ricca Chemical Company), and TLC plates (Baker-flex silica gel IB-F sheets 2.5×7.5 cm, J.T. Baker) were purchased from Thermo Fisher Scientific.

2.2 Microdroplet radiosynthesis of [¹⁸F]AMBF₃-TATE

The radiosynthesis was performed in droplets on microfluidic chips composed of Teflon-coated glass substrates. These simple chips serve as surrogates for more sophisticated electrowetting-on-dielectric (EWOD) chips [51–53] that could be used to perform fully-automated droplet synthesis. Details of fabrication are described in the Supplementary Information (Section 1). A simple temperature control system was assembled to heat and cool the glass chip (Figure 2). The detailed design of this subsystem is described in the Supplementary Information (Section 2).

[¹⁸F]AMBF₃-TATE was synthesized via an isotopic exchange process at a trifluoroborate group, similar to the SiFA methodology first introduced by Schirmacher and Jurkschat in 2006 [42]. To maximize the molar activity, the synthesis [55,58] was adapted to the droplet scale [50,59] to minimize the amount of precursor needed (Figure 3). Cyclotron-produced aqueous [¹⁸F]fluoride (up to 3.7 GBq [100 mCi], 100 μL) was deposited on the chip surface with addition of equal volume of MeCN (up to 60 μL) and 10 μL saline; the chip was then heated at 105°C for 2–3 min until only a tiny droplet remained. 5 nmol of TATE-AMBF₃ precursor, dissolved in pyridazine-HCl buffer / DMF (5 μL, 1M, pH 2.0–2.5), was loaded onto the chip and mixed with the dried residue. Next, the droplet was covered with a second chip placed Teflon-side down. This cover chip had narrow strips of tape adhered on the underside of 2 edges to provide a separation between the plates of 150 μm when assembled. The isotopic exchange reaction was carried out for 15 min at 90°C. After removing the top chip, the reaction was quenched by adding a 10 μL droplet of 5% aq. NH₃ to the reaction droplet. Next, the product was collected from the bottom chip by adding 20 μL of an EtOH/saline mixture (1:1 v/v) to the area where the droplet was in contact with the chip surface, and then transferring the diluted crude product with pipette into a clean vial. The process was then repeated with an additional 20 μL. Residual crude product was collected from the cover chip using a similar process.

For preclinical imaging purposes the collected product was purified and formulated for injection. It was first diluted with 5% aq. NH₃ quench solution to a volume of 2 mL and then slowly passed through the pre-conditioned C18 Sep-pack to trap [¹⁸F]AMBF₃-TATE. Next, the cartridge was washed with 4 mL of DI water. Finally, [¹⁸F]AMBF₃-TATE was eluted with 0.5 mL EtOH/saline mixture (1:1 v/v), and diluted to 10% EtOH with 2.0 mL saline. The resulting product was passed through a sterile 0.2 μm filter into a sterile empty glass vial. If more concentrated product was needed (i.e. to achieve at least 37–74 MBq/mL [1–2 mCi/mL] for imaging), the compound was instead formulated via an evaporation method. The [¹⁸F]AMBF₃-TATE was eluted from the cartridge with 2 mL EtOH into a glass vial with Teflon stir bar, and then the solvent was fully evaporated with nitrogen gas flow (7psi) under vacuum for 3–5 mins at 90°C (using an ELIXYS FLEX/CHEM radiosynthesizer, Sofie Biosciences, Inc., Culver City, CA, USA). Next, saline was added to redissolve the residue to the desired concentration and sterile filtration was performed.

Samples of final product or intermediate steps were analyzed via standard procedures to determine the performance of the synthesis (see Supplementary Information, Section 3).

2.3 Murine tumor models

To evaluate [¹⁸F]AMBF₃-TATE *in vivo*, NOD *scid* gamma (NSG) mice (n=4) were first engrafted with 1×10^7 AR42J cells (pancreatic NET model cell line naturally expressing SSTR2) in the left shoulder on day -7 and 1×10^5 RM1 cells (murine control cells, SSTR2-negative) in the right shoulder on day -3. This tumor inoculation protocol has been optimized to ensure similar tumor sizes of about 50 mm³ at day 0 for both cell lines. On day 0 [¹⁸F]FDG PET/CT imaging was performed to assess tumor viability and size. PET/CT imaging with [¹⁸F]AMBF₃-TATE and [⁶⁸Ga]Ga-DOTATATE were performed on day 1 and day 2, respectively. Across all imaging days, AR42J tumors were 56 ± 19 mm³ and RM1 tumors were 111 ± 59 mm³. (The RM1 tumors were larger due to their faster growth rate beginning at day 0.) To indicate well-preserved binding capability to the human receptor, RM1 cells stably transduced with human SSTR2 were used (RM1-hSSTR2).

AR42J cells were purchased from American Type Culture Collection (ATCC; Manassas, VA, USA), whereas the RM1 cells were kindly provided by Dr. Michel Sadelain (Memorial Sloan-Kettering Cancer Center, New York, USA). The cells were grown in Dulbecco's Modified Eagle's Medium (DMEM) with 4.5 g/L glucose, L-glutamine, sodium pyruvate (Cellgro, Corning Life Sciences) and 10% fetal bovine serum (Omega Scientific) at 37°C, 20% O₂ and 5% CO₂. For tumor injection, the cells were harvested and resuspended in a 1:1 mixture of PBS (Gibco Life Technologies) and Matrigel (Corning Life Sciences).

2.4 PET/CT imaging and biodistribution

PET/CT images were acquired using the integrated GENISYS 8 microPET/CT (Sofie Biosciences). It has a PET subsection optimized for mouse imaging with an energy window of 150–650 keV and peak sensitivity of approximately 14% at the center of field of view (FOV). The intrinsic detector spatial resolution is 1.5 mm FWHM in the transverse and axial directions. The CT section consists of a gantry and flywheel that uses a 50 kVp, 200 μA x-ray source and flat-panel detector. The CT acquires images in a continuous-rotation mode with 720 projections at 55 msec per projection, and reconstructed using a Feldkamp algorithm.

Tumor-bearing NSG mice underwent static imaging with [¹⁸F]FDG and [⁶⁸Ga]Ga-DOTATATE, and dynamic and static imaging with [¹⁸F]AMBF₃-TATE. For [¹⁸F]FDG imaging, the mice were fasted 4 hours prior to tracer injection. 0.74 MBq (20 μCi) of [¹⁸F]FDG were administered via tail vein injection. The mice were kept under 2% isoflurane anesthesia during the tracer uptake of 1 h and 10 min static PET imaging. For [⁶⁸Ga]Ga-DOTATATE imaging, the mice were injected with 1.1 MBq (30 μCi) of the tracer with conscious uptake of 1 h and 10 min static PET. For [¹⁸F]AMBF₃-TATE imaging, the mice were injected with 1.1 MBq (30 μCi) [¹⁸F]AMBF₃-TATE via a tail vein catheter at the beginning of 1 h dynamic PET scans, followed by 10 min static PET scans at 2 h. All mice received CT scans following each PET imaging. Image analysis was performed using AMIDE version 1.0.5 imaging software [60].

For determining [¹⁸F]AMBF₃-TATE dosimetry, male C57BL/6 mice (n=3) were injected with approximately 2.2 MBq (60 μCi) via a tail vein catheter at the beginning of 1 h

dynamic PET scans, followed by static PET scans at 2 h (10 min acquisition), 4 h (15 min acquisition) and 6 h (15 min acquisition). All mice received CT scans following each PET imaging. For improved soft tissue identification, for the last CT scan mice were injected via tail vein catheter with 100 μ L of Omnipaque 350 immediately before start of the CT scan, followed by an additional injection of 100 μ L during the first 30 s of scanning. Imaging biodistribution was confirmed by *ex vivo* analysis: each mouse was sacrificed following its last imaging time point and organs (brain, heart, lung, liver, kidneys, spleen, stomach, small intestine, large intestine, muscle, bone, bone marrow and blood) were collected, weighed and counted using a gamma counter (Cobra II Auto-Gamma, Packard Instrument Co., Meriden, USA) with decay correction to time of [18 F]AMBF₃-TATE injection. Data were normalized to mass of the organs.

2.5 [18 F]AMBF₃-TATE dosimetry

From [18 F]AMBF₃-TATE PET scans of 3 C57BL6 mice, the amount of radioactivity in selected organs was quantified and absorbed doses were calculated based on the respective time-integrated activity coefficients (TIACs; formerly known as residence times, RTs). The dose extrapolation to humans involved scaling the biodistributions and the subsequent calculation of the absorbed doses from the scaled biodistributions. The biodistribution scaling was performed by two alternative methods. Method 1 was based on the assumption that the TIAC for the same organ is the same in mice and humans [61,62]. Method 2 considered a relative mass scaling in which the TIAC value in a human organ is set equal to the TIAC value in the same animal organ multiplied by the ratio of whole body and the respective mass of the human and the animal organ[61,62].

TIACs were calculated using the software solution NUKFIT as described by Kletting *et al.*, choosing the optimal fit functions as proposed by the code [63]. TIAC values for bladder were calculated based on trapezoidal method. The absorbed dose calculation was performed for a selected group of organs using OLINDA/EXM v1.1 [64]. Details on the methodology used for extrapolating the mouse data to humans are provided in the Supplementary Information, Section 4.

2.6 Statistical Analysis

Data are presented as mean \pm standard deviation. All p values were determined with unpaired, two-tailed T tests and values less than 0.05 were considered to be statistically significant. Prism 6 (GraphPad Software) was used to calculate statistics and generate graphs.

3 Results

3.1 Microdroplet radiosynthesis of [18 F]AMBF₃-TATE

We initially performed low-radioactivity fluorination reactions and observed highly-reproducible performance with radiochemical conversion (as determined by a combination of radio-TLC and radio-HPLC analysis of the crude product) of $50 \pm 6\%$ (n=15), and non-isolated radiochemical yield (crude RCY) of $17 \pm 3\%$ (n=15). Full production runs were then performed, including cartridge purification and formulation, with up to 3.7 GBq [100

mCi] of activity. The RCY in these experiments was $16 \pm 1\%$ ($n=5$). Radiochemical purity was $>99\%$. A representative chromatogram is shown in the Supplementary Information (Section 5). The molar activity was determined for several syntheses ranging in starting activities from 0.185–1.85 GBq [5–50 mCi]. Molar activity was found to increase with starting activity, ranging from 37 to 185 GBq/ μmol [1 to 5 Ci/ μmol], all values decay-corrected to EOB (Figure S2).

3.2 Preclinical imaging

The preclinical biodistribution of [^{18}F]AMBF₃-TATE is summarized in Figure 4 and in the Supplementary Information (Figure S5). Highest tracer accumulation was observed in the bladder followed distantly by gastrointestinal tissues [55]. Bone retention was within range of background tissues lacking SSTR2, indicating little to no *in vivo* defluorination for [^{18}F]AMBF₃-TATE. [^{18}F]AMBF₃-TATE retention was approximately two-fold higher in SSTR2-high AR42J tumors than in SSTR2-low RM1 tumors ($3.99 \pm 0.75\%$ ID/g and $1.87 \pm 0.22\%$ ID/g, respectively; $p < 1.6 \times 10^{-3}$). Time-activity curves derived from PET imaging (see Supplementary Information, Figure S6) showed [^{18}F]AMBF₃-TATE saturation in AR42J tumors by 20 min, but a continuous decline in RM1 tumors after peaking at approximately 10 min. [^{68}Ga]Ga-DOTATATE uptake in the tumors at 1 hr post-injection ($3.94 \pm 0.53\%$ ID/g and $2.13 \pm 0.30\%$ ID/g, respectively; $p < 9.8 \times 10^{-4}$) was nearly identical to [^{18}F]AMBF₃-TATE. Results were confirmed with *ex vivo* gamma counter analysis of tissues after the last imaging time point. In contrast, [^{18}F]FDG imaging, a measure of tissue glucose metabolic activity, showed a reverse pattern with lower [^{18}F]FDG metabolism in AR42J tumors than RM1 tumors ($2.44 \pm 0.57\%$ ID/g and $5.25 \pm 2.14\%$ ID/g, respectively; $p < 4.4 \times 10^{-2}$).

3.3 Dosimetry analysis

Similarities in somatostatin peptide binding affinity between mouse and human SSTR2 suggest mouse dosimetry provides a good estimation for human dosimetry [65,66]. Absorbed doses for [^{18}F]AMBF₃-TATE in humans were extrapolated from mouse PET biodistribution data using two extrapolation methods, Method 1 and Method 2 (see Supplementary Information, Section 4). Organ TIAC values are summarized in Table 1 and a full list of the corresponding mean absorbed doses is provided in Table 2. The highest TIAC values were observed for the bladder and small intestine based on Method 1 (0.536 ± 0.021 h and 0.207 ± 0.019 h, respectively). Based on Method 2, the highest TIAC values were observed for the bladder, small intestine and bone marrow (0.536 ± 0.021 h, 0.237 ± 0.017 h and 0.030 ± 0.013 h, respectively). The highest absorbed dose value using the one-compartment voiding bladder model was 0.106 ± 0.003 mGy/MBq (Method 1) and 0.107 ± 0.004 mGy/MBq (Method 2) for the bladder. All other organs showed significantly lower absorbed dose values. Bladder was the dose-limiting organ and on average the maximum administered human activity limit is estimated as 472 MBq (Method 1) and 469 MBq (Method 2) (FDA Code of Federal Regulations 21CFR361.1). In addition, the effective dose per unit activity has been calculated. However, the quantity “effective dose” can only be applied to the description of stochastic radiation effects and organ absorbed doses of less than 1 Gy. The mean extrapolated effective doses are $1.26 \times 10^{-2} \pm 3.06 \times 10^{-4}$ mSv/MBq (Method 1) and $1.16 \times 10^{-2} \pm 1.53 \times 10^{-4}$ mSv/MBq (Method 2). This corresponds to

effective doses of 2.6 mSv (Method 1) and 2.4 mSv (Method 2) for an administered activity of 200 MBq, which is lower than that reported for current clinical ^{18}F - and ^{68}Ga -labeled PET tracers for imaging SSTR2-expressing tumors [20,67].

4 Discussion

4.1 Microdroplet radiosynthesis of $[^{18}\text{F}]\text{AMBF}_3\text{-TATE}$

The total synthesis duration (including purification and formulation) was 35–45 min, making this an attractive platform for on-demand production of $[^{18}\text{F}]\text{AMBF}_3\text{-TATE}$. It is expected that further developments of the microfluidic system could enable significant reductions of the synthesis time. For example, automation of reagent delivery steps [50], and automation of the purification and formulation process could reduce the time by up to 15 min and increase safety and simplicity of operation. While the yield was slightly lower than the 20–25% (uncorrected) yield reported by Liu *et al.* for the macroscale synthesis of $[^{18}\text{F}]\text{AMBF}_3\text{-TATE}$ [55], the microscale synthesis used 10x lower precursor (5 nmol vs 50 nmol). Notably, equally high molar activity could be achieved using much lower starting radioactivity (0.93–1.1 GBq [25–30 mCi] instead of 30–37 GBq [800–1000 mCi] to achieve ~110 GBq/ μmol [3 Ci/ μmol]). This is noteworthy insofar as the chip has significant potential for miniaturized production in a kit-like system [68]. Since the quantity and concentration of the tracer were sufficient for imaging, we did not perform significant optimization; however, in the Supplementary Information (Section 7), we report a detailed analysis of intermediate measurements during the synthesis and potential optimization strategies. While these yields are still a bit low, yields, purities, and molar activities are suitable to contemplate clinical use for human translation. In addition, the ease of use and the reproducibility in terms of yields and molar activity augur well for eventual clinical use.

By using portions of a large initial batch of $[^{18}\text{F}]\text{fluoride}$, or by producing small batches of $[^{18}\text{F}]\text{fluoride}$ throughout the day, we anticipate that radiosyntheses on the scale reported herein (i.e. up to ~3.7 GBq [100 mCi]) would be sufficient to supply patient doses throughout the day. Generation of $[^{18}\text{F}]\text{fluoride}$ throughout the day would have the advantage of ensuring similar molar activity for each batch of the tracer, but would require proximity to a cyclotron. In addition, the microdroplet approach may also be compatible with the concept of producing larger multi-dose batches. Though it is often assumed that microfluidic approaches are limited to only low activity levels, we should emphasize that this is not the case: whereas experiments here were limited to <3.7 GBq [100 mCi] for safety reasons, there are approaches to load significantly more activity into microdroplet reactions. One of us previously reported that ~30 GBq [~810 mCi] of $[^{18}\text{F}]\text{fluoride}$ can be concentrated into a volume of 5 μL [57], clearly opening up the possibility to use high levels of activity (sufficient for multiple patient doses) in microdroplet synthesis. Though it remains to be investigated in practice, mathematically, we would predict that the increase in scale from 3.7–30 GBq [100–800 mCi] would increase the molar activity 8-fold, assuming the amount of precursor is fixed at 5 nmol and that the batches of $[^{18}\text{F}]\text{fluoride}$ have similar molar activities. However, due to the increased proportion of $[^{18}\text{F}]\text{fluoride}$ relative to precursor, we would also predict that the RCY could decrease. To counteract this effect, the amount of precursor could be increased (e.g. from 5 to 40 nmol), while still achieving molar

activities in the range we report herein. As further evidence that scalable syntheses are well within the realm of possibility, it should also be noted that manual synthesis of [^{18}F]AMBF₃-TATE has been previously performed with 30–37 GBq [0.8–1.0 Ci] and 50 nmol precursor, resulting in 20–25% RCY and molar activities >111 GBq/ μmol [>3 Ci/ μmol] [55].

Finally, it should be appreciated that the BF₃ moiety can easily be connected to other molecules to create precursors for other radiolabeled peptides and dual-modality tracers [69,70] that can likely be labeled under identical or similar conditions. Microfluidic isotopic exchange labeling could therefore provide a route to a variety of ^{18}F -labeled compounds with simple production and high molar activity. Despite the low pH and relatively high reaction temperature, these conditions are not unusual in peptide synthesis as much more acidic conditions are typically used for resin cleavage e.g. 80% TFA, conc. HF, and during purification e.g. 1% TFA, pH 0, and are only slightly more acidic than methods commonly used in radiometallation of peptides (i.e., pH 3–4 and similar temperatures). Notably, several peptides and other small molecules have successfully been labeled with this approach [71]. While we recognize that not all functional groups (e.g. trityl groups, para-methoxybenzyl acetals) would survive these conditions, for the most part, standard peptides should be compatible. Further development and automation of the microdroplet labeling methods would benefit the development of this whole class of reactions.

4.2 Preclinical imaging and dosimetry

Preclinical biodistribution and dosimetry calculations for [^{18}F]AMBF₃-TATE showed significant potential for clinical use and was undertaken to further demonstrate that the radiotracer produced on the EWOD chip would provide clinically useful tracers with dosimetry that could be used to support clinical administration of this tracer as well as the further development of this method for labeling other peptide tracers. In particular, [^{18}F]AMBF₃-TATE showed very similar biodistribution to [^{68}Ga]Ga-DOTATATE in our experiments, and in comparisons with literature reports [55]. [^{18}F]AMBF₃-TATE tumor imaging corroborated with level of SSTR2 expression, but did not correlate with [^{18}F]FDG, suggesting these two tracers provide different information for therapeutic strategy and response monitoring. Dosimetry calculations showed lower effective dose per unit radioactivity than reported for current clinical ^{18}F - and ^{68}Ga -labeled PET tracers for imaging SSTR2-expressing tumors [20,67]. Since comparable performance to [^{68}Ga]Ga-DOTATATE (currently the clinical gold standard for imaging SSTR2) was achieved, these data suggest that further study of [^{18}F]AMBF₃-TATE, including evaluation in humans, is warranted.

5 Conclusions

We adapted the isotopic exchange based radiosynthesis of [^{18}F]AMBF₃-TATE to a droplet-based radiochemistry platform and could produce the injection-ready tracer in $16\pm 1\%$ (n=5) overall RCY (decay-corrected) in ~40 min. The small volume synthesis used minimal quantities of precursor (5 nmol), enabling high molar activity to be achieved, even starting from very little radioactivity. The BF₃ chemistry is very convenient, with straightforward

purification and formulation performed using solid-phase extraction on a C18 Sep-pak cartridge. Though only demonstrated at scales starting with <3.7 GBq [100 mCi] for safety reasons, it is possible to leverage technologies to concentrate [¹⁸F]fluoride ion for automated microdroplet synthesis to explore the possibility of scale-up to produce [¹⁸F]AMBF₃-TATE for multiple human doses.

Preclinical evaluation with [¹⁸F]AMBF₃-TATE in SSTR2 tumor models showed excellent contrast with surrounding tissues and comparable results to [⁶⁸Ga]Ga-DOTATATE. Due to the convenient synthetic method, favorable physical properties and scalability of fluorine-18 compared with gallium-68, and encouraging imaging and dosimetry, clinical translation of [¹⁸F]AMBF₃-TATE and further development of the microdroplet synthesis are warranted. We contend that the [¹⁸F]AMBF₃-TATE can be used for diagnosis and [¹⁷⁷Lu]Lu-DOTATATE can be used for therapy; eventual demonstration that [¹⁷⁷Lu]Lu-DOTATATE can block uptake of [¹⁸F]AMBF₃-TATE would be sufficient to fully qualify this for application as a companion diagnostic. Finally, while we have not addressed the possibility of boron neutron capture therapy (BNCT), the use of ¹⁰B-enriched AMBF₃ might constitute a promising approach that would qualify [¹⁸F]AMBF₃-TATE for diagnosis and [¹⁰B]AMBF₃-TATE for therapy in theranostic applications demanding a single molecule for both diagnosis and therapy.

Notably, we expect that other trifluoroborate conjugates of various other peptides could be labeled with fluorine-18 with high molar activity using the microdroplet approach in the same straightforward, kit-like manner, paving the way to the rapid development of novel ¹⁸F-labeled peptides for potential theranostic applications when paired with appropriate analogs labeled with therapeutic isotopes. Furthermore, the underlying microfluidic technology is anticipated to be compatible with other single-step peptide labeling methods (including organosilane conjugates labeled via isotopic exchange, NOTA conjugates labeled via chelation of [¹⁸F]AlF, etc.) or other more complex multi-step processes involving conjugate of modified peptides to ¹⁸F-labeled prosthetic groups. Leveraging the availability of fluorine-18 in high quantities, the microdroplet reactor is capable of producing sufficient quantities of ¹⁸F-labeled peptides for several human doses. Further efforts in automation of the overall droplet radiochemistry process will allow safe investigation of scaling activity levels above 3.7 GBq [100 mCi].

Supplementary Material

Refer to Web version on PubMed Central for supplementary material.

Acknowledgments

This work was supported in part by the National Institutes of Health (R21 EB015540, R21 AG049918, P30 CA016042, T32EB002101), the Caltech/UCLA Nanosystems Biology Cancer Center (NCI U54 CA151819), the Department of Energy Office of Science (DE-SC0012353) and the UCLA Foundation from a donation made by Ralph and Marjorie Crump for the Crump Institute for Molecular imaging. Funding for the synthesis of AMBF₃-TATE was provided by the CIHR (Canadian Institutes of Health Research). The authors thank Dr. Saman Sadeghi, Dr. Umesh Gangadharmath, and the staff of the UCLA Biomedical Cyclotron Facility for generously providing [¹⁸F]fluoride for some of these studies. The authors thank Liu Wei and Larry Pang of the Ahmanson Translational Imaging Division for assistance with preclinical imaging.

6 Abbreviations

NET	Neuroendocrine tumor
SSTR2	Somatostatin receptor type 2
RLT	Radioligand therapy
HPLC	High-performance liquid chromatography
FDA	Food and Drug Administration
TLC	Thin-layer chromatography
AAA	Advanced Accelerator Applications
EWOD	Electrowetting-on-dielectric
IEX	Isotopic exchange
RCY	Radiochemical yield
TIAC	Time-integrated activity coefficient
AMBF₃	ammoniomethyltrifluoroborate
DOTA	1,4,7,10-tetraazacyclododecane-1,4,7,10-tetraacetic acid
NOTA	1,4,7-triazacyclononane-1,4,7-trisacetic acid
FDG	2-fluoro-2-deoxy-D-glucose
RCP	Radiochemical purity
FWHM	Full-width half maximum
PET	Positron emission tomography

References

1. Bockisch A, Freudenberg LS, Schmidt D, Kuwert T. Hybrid Imaging by SPECT/CT and PET/CT: Proven Outcomes in Cancer Imaging. *Semin Nucl Med.* 2009; 39:276–89. DOI: 10.1053/j.semnuclmed.2009.03.003 [PubMed: 19497404]
2. Laforest R, Liu X. Image quality with non-standard nuclides in PET. *Q J Nucl Med Mol Imaging Off Publ Ital Assoc Nucl Med AIMN Int Assoc Radiopharmacol IAR Sect Soc Of.* 2008; 52:151–8.
3. Kemerink GJ, Visser MGW, Franssen R, Beijer E, Zamburlini M, Halders SGEA, et al. Effect of the positron range of ¹⁸F, ⁶⁸Ga and ¹²⁴I on PET/CT in lung-equivalent materials. *Eur J Nucl Med Mol Imaging.* 2011; 38:940–8. DOI: 10.1007/s00259-011-1732-1 [PubMed: 21287170]
4. Rischin D, Hicks RJ, Fisher R, Binns D, Corry J, Porceddu S, et al. Prognostic Significance of [18F]-Misonidazole Positron Emission Tomography–Detected Tumor Hypoxia in Patients With Advanced Head and Neck Cancer Randomly Assigned to Chemoradiation With or Without Tirapazamine: A Substudy of Trans-Tasman Radiation Oncology Group Study 98. 02. *J Clin Oncol.* 2006; 24:2098–104. DOI: 10.1200/JCO.2005.05.2878 [PubMed: 16648512]

5. Chang JM, Lee HJ, Goo JM, Lee H-Y, Lee JJ, Chung J-K, et al. False Positive and False Negative FDG-PET Scans in Various Thoracic Diseases. *Korean J Radiol.* 2006; 7:57–69. DOI: 10.3348/kjr.2006.7.1.57 [PubMed: 16549957]
6. Strauss LG. Fluorine-18 deoxyglucose and false-positive results: a major problem in the diagnostics of oncological patients. *Eur J Nucl Med.* 1996; 23:1409–15. DOI: 10.1007/BF01367602 [PubMed: 8781149]
7. Newton-Northup JR, Figueroa SD, Deutscher SL. Streamlined in vivo selection and screening of human prostate carcinoma avid phage particles for development of peptide based in vivo tumor imaging agents. *Comb Chem High Throughput Screen.* 2011; 14:9–21. DOI: 10.2174/1386207311107010009 [PubMed: 20958260]
8. Xiao W, Wang Y, Lau EY, Luo J, Yao N, Shi C, et al. The Use of One-Bead One-Compound Combinatorial Library Technology to Discover High-Affinity $\alpha v \beta 3$ Integrin and Cancer Targeting Arginine-Glycine-Aspartic Acid Ligands with a Built-in Handle. *Mol Cancer Ther.* 2010; 9:2714–23. DOI: 10.1158/1535-7163.MCT-10-0308 [PubMed: 20858725]
9. Lee S, Xie J, Chen X. Peptide-Based Probes for Targeted Molecular Imaging. *Biochemistry (Mosc).* 2010; 49:1364–76. DOI: 10.1021/bi901135x
10. Hong H, Goel S, Zhang Y, Cai W. Molecular Imaging with Nucleic Acid Aptamers. *Curr Med Chem.* 2011; 18:4195–205. [PubMed: 21838686]
11. Gong P, Shi B, Zheng M, Wang B, Zhang P, Hu D, et al. PEI protected aptamer molecular probes for contrast-enhanced in vivo cancer imaging. *Biomaterials.* 2012; 33:7810–7. DOI: 10.1016/j.biomaterials.2012.07.011 [PubMed: 22835645]
12. Gagnon MKJ, Hausner SH, Marik J, Abbey CK, Marshall JF, Sutcliffe JL. High-throughput in vivo screening of targeted molecular imaging agents. *Proc Natl Acad Sci U S A.* 2009; 106:17904–9. DOI: 10.1073/pnas.0906925106 [PubMed: 19815497]
13. Mansi L, Virgolini I. Diagnosis and therapy are walking together on radiopeptides' avenue. *Eur J Nucl Med Mol Imaging.* 2011; 38:605–12. DOI: 10.1007/s00259-011-1762-8 [PubMed: 21365250]
14. Banerjee SR, Pomper MG. Clinical applications of Gallium-68. *Appl Radiat Isot.* 2013; 76:2–13. DOI: 10.1016/j.apradiso.2013.01.039 [PubMed: 23522791]
15. Avril N, Menzel M, Dose J, Schelling M, Weber W, Jänicke F, et al. Glucose Metabolism of Breast Cancer Assessed by 18F-FDG PET: Histologic and Immunohistochemical Tissue Analysis. *J Nucl Med.* 2001; 42:9–16. [PubMed: 11197987]
16. Alberini J-L, Edeline V, Giraudet AL, Champion L, Paulmier B, Madar O, et al. Single photon emission tomography/computed tomography (SPET/CT) and positron emission tomography/computed tomography (PET/CT) to image cancer. *J Surg Oncol.* 2011; 103:602–6. DOI: 10.1002/jso.21695 [PubMed: 21480254]
17. Pecking AP, Bellet D, Alberini JL. Immuno-SPET/CT and immuno-PET/CT: a step ahead to translational imaging. *Clin Exp Metastasis.* 2012; 29:847–52. DOI: 10.1007/s10585-012-9501-5 [PubMed: 22760521]
18. Öberg K. Diagnostic work-up of gastroenteropancreatic neuroendocrine tumors. *Clinics.* 2012; 67:109–12. DOI: 10.6061/clinics/2012(Sup01)18 [PubMed: 22584714]
19. Kwekkeboom DJ, Kam BL, Essen M, van Teunissen JJM, Eijck CHJ, van Valkema R, et al. Somatostatin receptor-based imaging and therapy of gastroenteropancreatic neuroendocrine tumors. *Endocr Relat Cancer.* 2010; 17:R53–73. DOI: 10.1677/ERC-09-0078 [PubMed: 19995807]
20. Walker RC, Smith GT, Liu E, Moore B, Clanton J, Stabin M. Measured Human Dosimetry of 68Ga-DOTATATE. *J Nucl Med.* 2013; 54:855–60. DOI: 10.2967/jnumed.112.114165 [PubMed: 23516312]
21. van Vliet EI, Teunissen JJM, Kam BLR, de Jong M, Krenning EP, Kwekkeboom DJ. Treatment of Gastroenteropancreatic Neuroendocrine Tumors with Peptide Receptor Radionuclide Therapy. *Neuroendocrinology.* 2013; 97:74–85. DOI: 10.1159/000335018 [PubMed: 22237390]
22. Singla S, Gupta S, Reddy RM, Durgapal P, Bal CS. 68Ga-DOTA-NOC PET and Peptide Receptor Radionuclide Therapy in Management of Bilateral Ovarian Metastases from Gastrointestinal Carcinoid. *Jpn J Clin Oncol.* 2012; 42:1202–6. DOI: 10.1093/jjco/hys172 [PubMed: 23107835]

23. Yu Z, Ananias HJK, Carlucci G, Hoving HD, Helfrich W, Dierckx RAJO, et al. An update of radiolabeled bombesin analogs for gastrin-releasing peptide receptor targeting. *Curr Pharm Des.* 2013; 19:3329–41. [PubMed: 23431995]
24. Müller C. Folate-Based Radiotracers for PET Imaging—Update and Perspectives. *Molecules.* 2013; 18:5005–31. DOI: 10.3390/molecules18055005 [PubMed: 23629756]
25. Betzel T, Müller C, Groehn V, Müller A, Reber J, Fischer CR, et al. Radiosynthesis and Preclinical Evaluation of 3'-Aza-2'-[18F]fluorofolic Acid: A Novel PET Radiotracer for Folate Receptor Targeting. *Bioconjug Chem.* 2013; 24:205–14. DOI: 10.1021/bc300483a [PubMed: 23273015]
26. Fischer CR, Müller C, Reber J, Müller A, Krämer SD, Ametamey SM, et al. [18F]Fluoro-Deoxy-Glucose Folate: A Novel PET Radiotracer with Improved in Vivo Properties for Folate Receptor Targeting. *Bioconjug Chem.* 2012; 23:805–13. DOI: 10.1021/bc200660z [PubMed: 22372827]
27. Muller C. Folate based radiopharmaceuticals for imaging and therapy of cancer and inflammation. *Curr Pharm Des.* 2012; 18:1058–83. [PubMed: 22272825]
28. Segal EI, Low PS. Tumor detection using folate receptor-targeted imaging agents. *Cancer Metastasis Rev.* 2008; 27:655. doi: 10.1007/s10555-008-9155-6 [PubMed: 18523731]
29. Low PS, Henne WA, Doorneweerd DD. Discovery and Development of Folic-Acid-Based Receptor Targeting for Imaging and Therapy of Cancer and Inflammatory Diseases. *Acc Chem Res.* 2008; 41:120–9. DOI: 10.1021/ar7000815 [PubMed: 17655275]
30. Wan W, Guo N, Pan D, Yu C, Weng Y, Luo S, et al. First Experience of 18F-Alfatide in Lung Cancer Patients Using a New Lyophilized Kit for Rapid Radiofluorination. *J Nucl Med.* 2013; 54:691–8. DOI: 10.2967/jnumed.112.113563 [PubMed: 23554506]
31. Choi H, Phi JH, Paeng JC, Kim S-K, Lee Y-S, Jeong JM, et al. Imaging of Integrin $\alpha\beta3$ Expression Using 68Ga-RGD Positron Emission Tomography in Pediatric Cerebral Infarct. *Mol Imaging.* 2013; 12 7290.2012.00036. doi: 10.2310/7290.2012.00036
32. Beer AJ, Haubner R, Sarbia M, Goebel M, Luderschmidt S, Grosu AL, et al. Positron Emission Tomography Using [18F]Galacto-RGD Identifies the Level of Integrin $\alpha\beta3$ Expression in Man. *Clin Cancer Res.* 2006; 12:3942–9. DOI: 10.1158/1078-0432.CCR-06-0266 [PubMed: 16818691]
33. Vlahov IR, Leamon CP. Engineering Folate Drug Conjugates to Target Cancer: From Chemistry to Clinic. *Bioconjug Chem.* 2012; 23:1357–69. DOI: 10.1021/bc2005522 [PubMed: 22667324]
34. Teng L, Xie J, Teng L, Lee RJ. Clinical translation of folate receptor-targeted therapeutics. *Expert Opin Drug Deliv.* 2012; 9:901–8. DOI: 10.1517/17425247.2012.694863 [PubMed: 22663189]
35. Pozsgai E, Schally AV, Halmos G, Rick F, Bellyei S. The Inhibitory Effect of a Novel Cytotoxic Somatostatin Analogue AN-162 on Experimental Glioblastoma. *Horm Metab Res.* 2010; 42:781–6. DOI: 10.1055/s-0030-1261955 [PubMed: 20665426]
36. Hohla F, Buchholz S, Schally AV, Krishan A, Rick FG, Szalontay L, et al. Targeted cytotoxic somatostatin analog AN-162 inhibits growth of human colon carcinomas and increases sensitivity of doxorubicin resistant murine leukemia cells. *Cancer Lett.* 2010; 294:35–42. DOI: 10.1016/j.canlet.2010.01.018 [PubMed: 20156671]
37. Hanaoka H, Tominaga H, Yamada K, Paudyal P, Iida Y, Watanabe S, et al. Evaluation of 64Cu-labeled DOTA-D-Phe(1)-Tyr(3)-octreotide (64Cu-DOTA-TOC) for imaging somatostatin receptor-expressing tumors. *Ann Nucl Med.* 2009; 23:559–67. DOI: 10.1007/s12149-009-0274-0 [PubMed: 19504168]
38. Boswell CA, Sun X, Niu W, Weisman GR, Wong EH, Rheingold AL, et al. Comparative in Vivo Stability of Copper-64-Labeled Cross-Bridged and Conventional Tetraazamacrocyclic Complexes. *J Med Chem.* 2004; 47:1465–74. DOI: 10.1021/jm030383m [PubMed: 14998334]
39. Bass LA, Wang M, Welch MJ, Anderson CJ. In Vivo Transchelation of Copper-64 from TETA-Octreotide to Superoxide Dismutase in Rat Liver. *Bioconjug Chem.* 2000; 11:527–32. DOI: 10.1021/bc9901671 [PubMed: 10898574]
40. Zhan C-G, Dixon DA. Hydration of the Fluoride Anion: Structures and Absolute Hydration Free Energy from First-Principles Electronic Structure Calculations. *J Phys Chem A.* 2004; 108:2020–9. DOI: 10.1021/jp0311512
41. Cai L, Lu S, Pike VW. Chemistry with [18F]Fluoride Ion. *Eur J Org Chem.* 2008; 2008:2853–73. DOI: 10.1002/ejoc.200800114

42. Schirmacher R, Bradtmöller G, Schirmacher E, Thews O, Tillmanns J, Siessmeier T, et al. 18F-Labeling of Peptides by means of an Organosilicon-Based Fluoride Acceptor. *Angew Chem Int Ed*. 2006; 45:6047–50. DOI: 10.1002/anie.200600795
43. Niedermoser S, Chin J, Wängler C, Kostikov A, Bernard-Gauthier V, Vogler N, et al. In Vivo Evaluation of 18F-SiFAlin-Modified TATE: A Potential Challenge for 68Ga-DOTATATE, the Clinical Gold Standard for Somatostatin Receptor Imaging with PET. *J Nucl Med*. 2015; 56:1100–5. DOI: 10.2967/jnumed.114.149583 [PubMed: 25977461]
44. McBride WJ, Sharkey RM, Karacay H, D'Souza CA, Rossi EA, Laverman P, et al. A Novel Method of 18F Radiolabeling for PET. *J Nucl Med*. 2009; 50:991–8. DOI: 10.2967/jnumed.108.060418 [PubMed: 19443594]
45. Laverman P, D'Souza CA, Eek A, McBride WJ, Sharkey RM, Oyen WJG, et al. Optimized labeling of NOTA-conjugated octreotide with F-18. *Tumor Biol*. 2012; 33:427–34. DOI: 10.1007/s13277-011-0250-x
46. McBride WJ, Sharkey RM, Goldenberg DM. Radiofluorination using aluminum-fluoride (Al18F). *EJNMMI Res*. 2013; 3:36.doi: 10.1186/2191-219X-3-36 [PubMed: 23651690]
47. Liu Z, Li Y, Lozada J, Schaffer P, Adam MJ, Ruth TJ, et al. Stoichiometric Leverage: Rapid 18F-Aryltrifluoroborate Radiosynthesis at High Specific Activity for Click Conjugation. *Angew Chem Int Ed*. 2013; 52:2303–7. DOI: 10.1002/anie.201208551
48. Rensch C, Jackson A, Lindner S, Salvamoser R, Samper V, Riese S, et al. Microfluidics: A Groundbreaking Technology for PET Tracer Production? *Molecules*. 2013; 18:7930–56. DOI: 10.3390/molecules18077930 [PubMed: 23884128]
49. Pascali G, Watts P, Salvadori P. Microfluidics in radiopharmaceutical chemistry. *Nucl Med Biol*. 2013; 40:776–87. DOI: 10.1016/j.nucmedbio.2013.04.004 [PubMed: 23684316]
50. Keng PY, van Dam RM. Digital Microfluidics: A New Paradigm for Radiochemistry. *Mol Imaging*. 2015; 14:579–94.
51. Keng PY, Chen S, Ding H, Sadeghi S, Shah GJ, Dooraghi A, et al. Micro-chemical synthesis of molecular probes on an electronic microfluidic device. *Proc Natl Acad Sci*. 2012; 109:690–5. DOI: 10.1073/pnas.1117566109 [PubMed: 22210110]
52. Javed MR, Chen S, Kim H-K, Wei L, Czernin J, Kim C-J, et al. Efficient Radiosynthesis of 3'-Deoxy-3'-18F-Fluorothymidine Using Electrowetting-on-Dielectric Digital Microfluidic Chip. *J Nucl Med*. 2014; 55:321–8. DOI: 10.2967/jnumed.113.121053 [PubMed: 24365651]
53. Javed MR, Chen S, Lei J, Collins J, Sergeev M, Kim H-K, et al. High yield and high specific activity synthesis of [18F]fallypride in a batch microfluidic reactor for micro-PET imaging. *Chem Commun*. 2014; 50:1192–4. DOI: 10.1039/C3CC47616B
54. Chen S, Javed MR, Kim H-K, Lei J, Lazari M, Shah GJ, et al. Radiolabelling diverse positron emission tomography (PET) tracers using a single digital microfluidic reactor chip. *Lab Chip*. 2014; 14:902–10. DOI: 10.1039/C3LC51195B [PubMed: 24352530]
55. Liu Z, Pourghiasian M, Bénard F, Pan J, Lin K-S, Perrin DM. Preclinical Evaluation of a High-Affinity 18F-Trifluoroborate Octreotate Derivative for Somatostatin Receptor Imaging. *J Nucl Med*. 2014; 55:1499–505. DOI: 10.2967/jnumed.114.137836 [PubMed: 24970911]
56. Herrmann K, Czernin J, Wolin EM, Gupta P, Barrio M, Gutierrez A, et al. Impact of 68Ga-DOTATATE PET/CT on the Management of Neuroendocrine Tumors: The Referring Physician's Perspective. *J Nucl Med*. 2015; 56:70–5. DOI: 10.2967/jnumed.114.148247 [PubMed: 25500825]
57. Elizarov AM, van Dam RM, Shin YS, Kolb HC, Padgett HC, Stout D, et al. Design and Optimization of Coin-Shaped Microreactor Chips for PET Radiopharmaceutical Synthesis. *J Nucl Med*. 2010; 51:282–7. DOI: 10.2967/jnumed.109.065946 [PubMed: 20124050]
58. Liu Z, Lin K-S, Bénard F, Pourghiasian M, Kiesewetter DO, Perrin DM, et al. One-step 18F labeling of biomolecules using organotrifluoroborates. *Nat Protoc*. 2015; 10:1423–32. DOI: 10.1038/nprot.2015.090 [PubMed: 26313478]
59. Keng, PY., Sergeev, M., van Dam, RM. Advantages of Radiochemistry in Microliter Volumes. In: Kuge, Y., Shiga, T., Tamaki, N., editors. *Perspect Nucl Med Mol Diagn Integr Ther*. Springer; Japan: 2016. p. 93-111.
60. Loening AM, Gambhir SS. AMIDE: a free software tool for multimodality medical image analysis. *Mol Imaging*. 2003; 2:131–7. [PubMed: 14649056]

61. Repetto-Llamazares AHV, Larsen RH, Mollatt C, Lassmann M, Dahle J. Biodistribution and Dosimetry of ¹⁷⁷Lu-tetumab, a New Radioimmunoconjugate for Treatment of Non-Hodgkin Lymphoma. *Curr Radiopharm.* 2013; 6:20–7. DOI: 10.2174/1874471011306010004 [PubMed: 23256748]
62. Sparks, RB., Aydogan, B. Comparison of the Effectiveness of Some Common Animal Data Scaling Techniques in Estimating Human Radiation Dose. *Proc. Sixth Int. Radiopharm. Dosim. Symp;* Gatlinburg, TN: Oak Ridge Associated Universities, TN (United States); 1996. p. 705-16.
63. Kletting P, Schimmel S, Kestler HA, Hänscheid H, Luster M, Fernández M, et al. Molecular radiotherapy: The NUKFIT software for calculating the time-integrated activity coefficient. *Med Phys.* 2013; 40:102504.doi: 10.1118/1.4820367 [PubMed: 24089925]
64. Stabin MG, Sparks RB, Crowe E. OLINDA/EXM: The Second-Generation Personal Computer Software for Internal Dose Assessment in Nuclear Medicine. *J Nucl Med.* 2005; 46:1023–7. [PubMed: 15937315]
65. Bruns C, Raulf F, Hoyer D, Schloos J, Lübbert H, Weckbecker G. Binding properties of somatostatin receptor subtypes. *Metabolism.* 1996; 45:17–20. DOI: 10.1016/S0026-0495(96)90072-4 [PubMed: 8769372]
66. Yamada Y, Post SR, Wang K, Tager HS, Bell GI, Seino S. Cloning and functional characterization of a family of human and mouse somatostatin receptors expressed in brain, gastrointestinal tract, and kidney. *Proc Natl Acad Sci.* 1992; 89:251–5. [PubMed: 1346068]
67. Dubash SR, Keat N, Mapelli P, Twyman F, Carroll L, Kozlowski K, et al. Clinical Translation of a Click-Labeled ¹⁸F-Octreotate Radioligand for Imaging Neuroendocrine Tumors. *J Nucl Med.* 2016; 57:1207–13. DOI: 10.2967/jnumed.115.169532 [PubMed: 27173162]
68. Keng, PY., Esterby, M., van Dam, RM. Emerging Technologies for Decentralized Production of PET Tracers. In: Hsieh, C-H., editor. *Positron Emiss Tomogr - Curr Clin Res Asp.* Rijeka, Croatia: InTech; 2012. p. 153-82.
69. Liu Z, Pourghasian M, Radtke MA, Lau J, Pan J, Dias GM, et al. An Organotrifluoroborate for Broadly Applicable One-Step ¹⁸F-Labeling. *Angew Chem Int Ed.* 2014; 53:11876–80. DOI: 10.1002/anie.201406258
70. Pourghasian M, Liu Z, Pan J, Zhang Z, Colpo N, Lin K-S, et al. ¹⁸F-AmBF₃-MJ9: A novel radiofluorinated bombesin derivative for prostate cancer imaging. *Bioorg Med Chem.* 2015; 23:1500–6. DOI: 10.1016/j.bmc.2015.02.009 [PubMed: 25757604]
71. Bernard-Gauthier V, Bailey JJ, Liu Z, Wängler B, Wängler C, Jurkschat K, et al. From Unorthodox to Established: The Current Status of ¹⁸F-Trifluoroborate- and ¹⁸F-SiFA-Based Radiopharmaceuticals in PET Nuclear Imaging. *Bioconjug Chem.* 2016; 27:267–79. DOI: 10.1021/acs.bioconjchem.5b00560 [PubMed: 26566577]

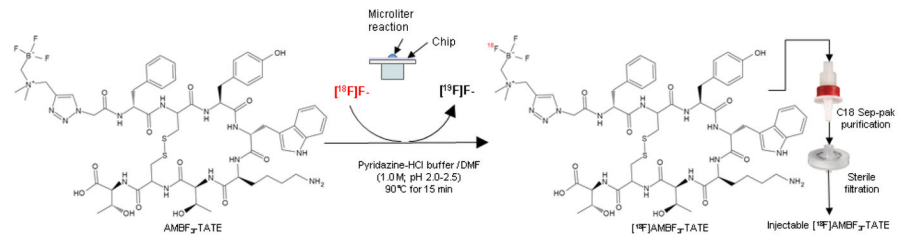


Fig. 1. Radiosynthesis of $[^{18}\text{F}]\text{AMBF}_3\text{-TATE}$ via isotopic exchange on a microfluidic chip

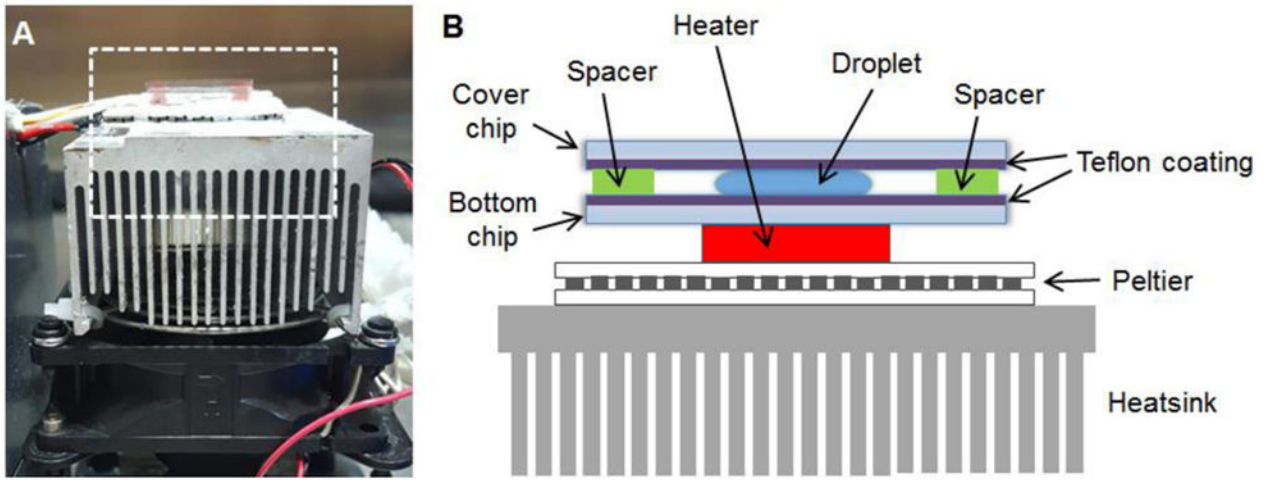


Fig. 2.
 (A) Photograph of heating setup and microfluidic reaction chip. (B) Schematic of the chip and heating setup

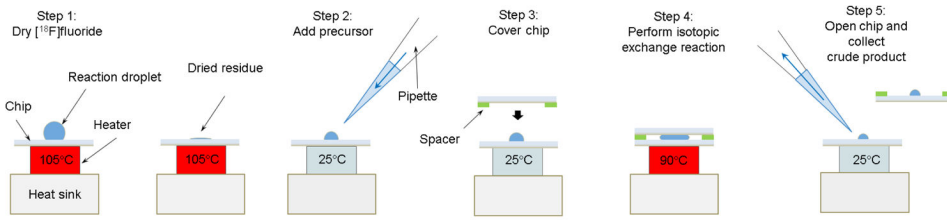


Fig. 3. Schematic of the sequence of operations to perform the microdroplet radiosynthesis of ^{18}F AMBF₃-TATE on the chip

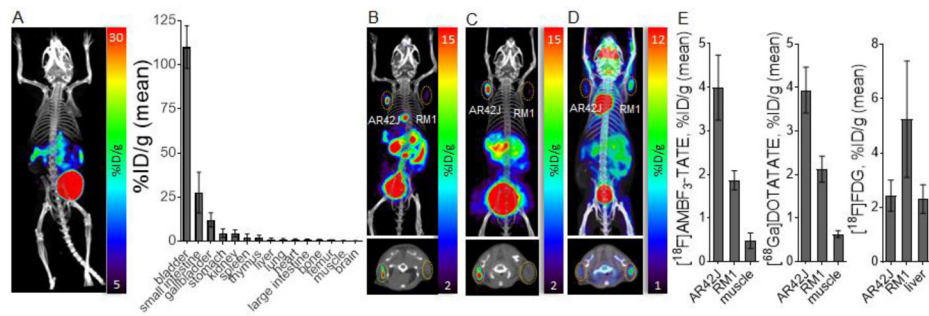


Fig. 4.

MicroPET/CT imaging. (A) MIP image and tissue biodistribution of 1.1 MBq injection of $[^{18}\text{F}]\text{AMBF}_3\text{-TATE}$ in C57BL6 mouse, $n=3$. MIP image (top) and transverse slice (bottom) of (B) 1.1 MBq injection of $[^{18}\text{F}]\text{AMBF}_3\text{-TATE}$, (C) 1.1 MBq injection of $[^{68}\text{Ga}]\text{Ga-DOTATATE}$ and (D) 0.74 MBq injection of $[^{18}\text{F}]\text{FDG}$ of the same NSG mouse engrafted with SSTR2-positive (AR42J; left) and SSTR2-negative (RM1; right) tumor cells. (E) Region-of-interest analysis of PET images, $n=4$. Images were acquired for 10 min under 2% isoflurane anesthesia at 1 h post-injection of the PET tracer. Error bars are standard deviations. Tumors are delineated in dashed circles. MIP = maximum intensity projection.

Table 1

Mean time-integrated activity coefficient (TIAC) values for the several organs scaled to humans

Target Organs	Mean TIAC (h)		Standard deviations (h)	
	Method 1	Method 2	Method 1	Method 2
Bladder	5.36E-01	5.36E-01	2.14E-02	2.14E-02
Bone marrow	1.77E-02	2.95E-02	7.99E-03	1.33E-02
Brain	1.73E-03	2.10E-03	4.30E-04	7.10E-04
Gallbladder content	5.34E-03	2.05E-02	4.02E-03	1.58E-02
Heart content	2.74E-03	6.01E-03	1.78E-04	1.08E-03
Heart wall	3.04E-04	6.67E-04	1.97E-05	1.19E-04
Kidneys	4.23E-02	1.27E-02	5.77E-03	2.05E-03
Liver	2.07E-02	1.45E-02	5.56E-03	3.53E-03
Lungs	2.99E-03	6.62E-03	4.89E-04	1.93E-03
Small intestine	2.07E-01	2.37E-01	1.91E-02	1.72E-02
Spleen	1.88E-03	2.95E-03	1.45E-03	1.62E-03
Stomach	3.50E-02	4.94E-03	4.49E-03	3.17E-04
Cortical bone	1.62E-02	1.52E-02	1.23E-02	1.20E-02
Trabecular bone	7.97E-03	7.50E-03	6.06E-03	5.90E-03
Remainder of body	4.70E-01	4.72E-01	9.62E-02	7.50E-02

Table 2

Mean absorbed dose coefficient values of the organs and the respective standard deviations for both methods using a one-compartment voiding bladder model.

Target Organ	Mean absorbed dose coefficients of the organs (mGy/MBq)		Standard deviations (mGy/MBq)	
	Method 1	Method 2	Method 1	Method 2
Adrenals	4.44E-03	3.91E-03	3.96E-04	4.62E-04
Brain	8.40E-04	9.27E-04	1.11E-04	1.58E-04
Breasts	2.20E-03	2.21E-03	3.75E-04	3.12E-04
Gallbladder Wall	1.45E-02	3.80E-02	6.59E-03	2.49E-02
LLI Wall	9.08E-03	9.49E-03	2.20E-04	1.97E-04
Small Intestine	4.54E-02	5.12E-02	3.25E-03	2.85E-03
Stomach Wall	1.71E-02	6.14E-03	1.90E-03	3.38E-04
ULI Wall	1.14E-02	1.24E-02	1.73E-04	2.89E-04
Heart Wall	2.63E-03	3.43E-03	2.12E-04	3.03E-04
Kidneys	2.88E-02	1.09E-02	3.32E-03	1.10E-03
Liver	4.85E-03	4.22E-03	7.34E-04	5.61E-04
Lungs	2.15E-03	2.72E-03	2.48E-04	4.53E-04
Muscle	3.96E-03	3.97E-03	3.67E-04	3.27E-04
Ovaries	1.04E-02	1.11E-02	1.15E-04	1.73E-04
Pancreas	5.51E-03	4.68E-03	5.20E-04	5.75E-04
Red Marrow	5.43E-03	6.26E-03	5.64E-04	9.45E-04
Osteogenic Cells	6.40E-03	6.78E-03	1.96E-04	2.95E-04
Skin	2.45E-03	2.44E-03	3.21E-04	2.66E-04
Spleen	5.35E-03	5.54E-03	1.28E-03	1.52E-03
Testes	4.60E-03	4.63E-03	3.87E-04	2.93E-04
Thymus	2.62E-03	2.71E-03	4.56E-04	3.72E-04
Thyroid	2.53E-03	2.57E-03	4.65E-04	3.75E-04
Urinary Bladder Wall	1.06E-01	1.07E-01	3.00E-03	3.51E-03
Uterus	1.36E-02	1.41E-02	1.53E-04	2.00E-04